CHEMISTRY OF MATERIALS

pubs.acs.org/cm

Article

Vibrational Stark Effect Mapping of Polaron Delocalization in Chemically Doped Conjugated Polymers

Dane A. Stanfield, Zerina Mehmedović, and Benjamin J. Schwartz*

Cite This: https://doi.org/10.1021/acs.chemmater.1c02934

Read Online

ACCESS | Metrics & More | Article Recommendations | Supporting Information

ABSTRACT: The nitrile vibrational modes of the 2,3,5,6-tetrafluoro-7,7,8,8-tetracyanoquinodimethane (F_4TCNQ) anion occur across a range of different frequencies in doped conjugated polymers. We show that these shifts can be understood as resulting from the vibrational Stark effect. F_4TCNQ^- serves as a sensitive vibrational Stark probe, and its nitrile stretches provide a direct readout of the locally experienced electric fields from the nearby polaron on the doped polymer backbone. The shift of the F_4TCNQ^- B_{1u} mode and broadening of the B_{2u} mode in doped poly(3-hexylthiophene-2,5-diyl) (P3HT) confirm that the dopant anion's long axis is oriented perpendicular to the P3HT backbone. The magnitude of the vibrational shifts prove that the anion−polaron distance in F_4TCNQ^--doped P3HT films is ∼6 Å. We also show that the intrachain polaron coherence can be varied over a range spanning 6 to about 7.5 P3HT monomer units by controlling the local polymer order and crystallinity. At the highest degree of local order, polaron delocalization is limited by the minimum intrinsic strength of the anion−polaron Coulombic interaction. This work provides the first direct experimental measurement of polaron delocalization in doped conjugated polymer films and verifies theoretical models relating polaron coherence to the shape of the doped polymer's mid-IR electronic absorption spectrum.

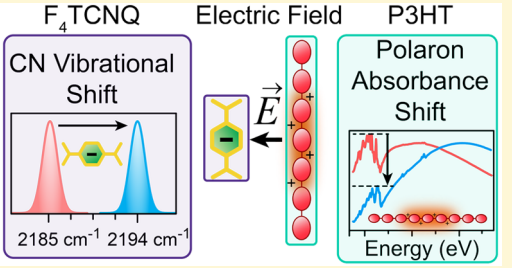

1. INTRODUCTION

Chemical doping of conjugated polymers has emerged as a viable method for tuning the electronic properties of organic electronic devices such as thermoelectrics and photovoltaics.[1−5] In the simplest case, p-type doping of polymer-based semiconductors can be achieved through the introduction of strong oxidizing agents whose LUMO levels are energetically lower than the HOMO levels of the semiconducting polymer. This leads to doping via integer charge transfer (ICT), where each dopant molecule removes an electron from the polymer π-system, producing both a cationic hole that can delocalize along the conjugated backbone (also termed a polaron) and a counterion formed from the reduced dopant.

A variety of recent work has suggested that the ICT-separated hole and dopant counterion Coulombic interaction plays a fundamental role in determining the carrier behavior in doped conjugated polymers: the stronger the Coulombic interaction, the lower the polaron delocalization and carrier mobility.[6−14] The experimental evidence for charge carrier−counterion interactions, however, is indirect, based mostly on features observed in the polaron mid-IR absorption spectrum. One of the goals of this paper is to provide a means by which to directly measure the local electric fields experienced by polarons and dopant counterions in doped conjugated polymers.

The approach we take is based on the fact that the strength of the Coulombic interaction between polarons on the conjugated polymer backbone and dopant counterions is actually recorded in the vibrational spectra of certain dopant anions. Our first hint that this might be possible comes from previous work by both our group[15] and others[16−25] who have used the nitrile stretching vibrational spectrum of the 2,3,5,6-tetrafluoro-7,7,8,8-tetracyanoquinodimethane (F_4TCNQ) dopant as a diagnostic tool for tracking the doping mechanism in conjugated polymers, which takes place either via ICT or by the formation of charge transfer complexes (CTCs). Nitrile stretching modes have the advantage that they occur in a mid-IR spectral "window" where no other molecular vibrations appear, so that they are relatively easy to measure and characterize. In the context of studying CTCs, the nitrile stretching modes of the neutral F_4TCNQ molecule undergo a predictable softening in their resonant vibrational energy that is roughly proportional to the oxidation state of the molecule. As a result, vibrational absorption at intermediate energies between the neutral and anionically charged species is understood to represent a fractional charge transfer state for the dopant molecule.

The sensitivity of dopant vibrations to the local polymer environment also can be seen in work from Hase et al.,[26] who

Received: August 25, 2021
Revised: October 8, 2021

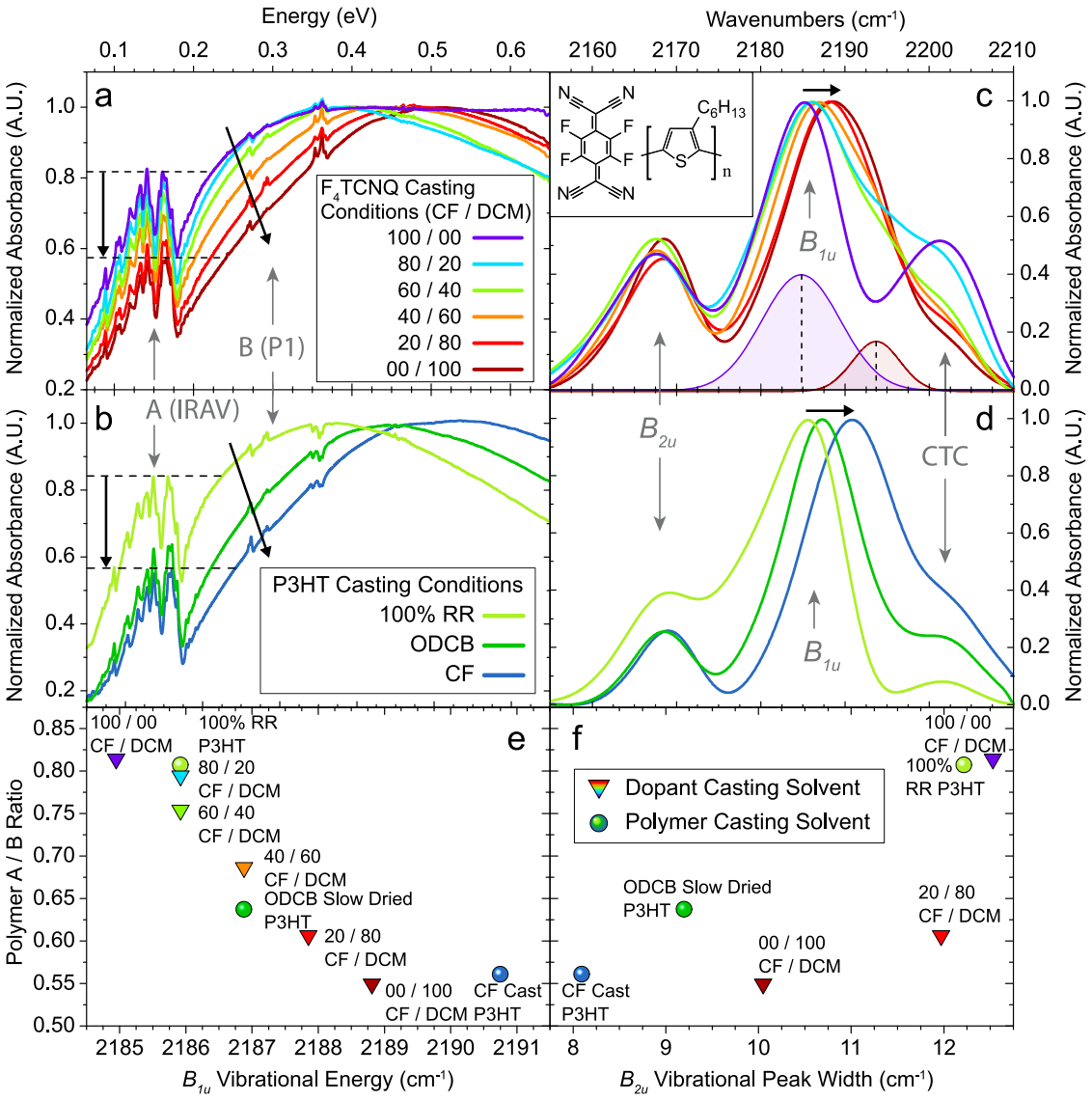

Figure 1. (a) Normalized mid-IR electronic absorption spectra for P3HT films sequentially doped with F_4TCNQ (1 mg mL^{-1}) from solvent blends composed of CF and DCM. (b) Normalized mid-IR electronic absorption spectra of doped P3HT films where the initial films are created to have a range of crystallinities and then subsequently doped with F_4TCNQ (1 mg mL^{-1}) from DCM. For the blue and dark green curves, commercially available P3HT with a regioregularity of 91−94% was used, and the relative film crystallinity was controlled by varying the drying time of the casting solvent. A specially synthesized batch of P3HT with virtually 100% regioregularity was cast from ODCB to obtain the most ordered conditions shown in light green (see the Supporting Information for X-ray-based structural characterization). The A/B spectral ratio (see text) for both panels a and b can be estimated on the vertical axis by following the horizontal dashed lines. (c) F_4TCNQ nitrile stretch vibrational spectra of the doped films in panel a (also directly visible in panel a as tiny peaks near 0.27 eV). The shaded Gaussians correspond to peak fits for the conditions using 100% CF as the doping solvent, reduced to 0.3 intensity for ease of viewing (see the Supporting Information for fitting details). (d) F_4TCNQ nitrile stretching vibrational spectra of the doped films in panel b. (e) Scatter plot displaying the experimentally measured A/B ratio for the samples in panels a and b plotted against the vibrational energy of the F_4TCNQ^- B_{1u} mode. (f) Scatter plot displaying the A/B ratio for all the samples in panels a and b plotted against the peak width of the F_4TCNQ^- B_{2u} vibrational mode.

recently studied the nitrile stretching vibrational spectrum of the F_4TCNQ radical anion inside blend-doped films of poly(3-hexylthiophene-2,5-diyl) (P3HT). These workers showed that the amplitude of certain F_4TCNQ^- vibrational features can change quite dramatically (and even disappear) when the doped films are subjected to thermal annealing cycles. This demonstrates that the precise vibrational spectrum of the F_4TCNQ dopant anion is in fact dependent on the local structural morphology. As a result, it has become increasingly clear that the F_4TCNQ vibrational spectrum can change in subtle ways as a result of the charge state of the molecule and the local structural morphology in which it resides.

In this paper, we provide a comprehensive picture of the Coulombic interactions in F_4TCNQ-doped P3HT films that links the behavior of the F_4TCNQ nitrile vibrational spectrum to the degree of polaron delocalization in the doped polymer, the local structural disorder, and the polaron-dopant Coulombic interactions that ultimately control the charge carrier mobility. We show that the counterion vibrational spectrum is directly influenced by the local electric field emanating from the nearby hole and thus can serve as an exquisite reporter of the degree of polaron delocalization on the nearby conjugated polymer.

https://doi.org/10.1021/acs.chemmater.1c02934
Chem. Mater. XXXX, XXX, XXX−XXX

We then argue that the behavior of the F_4TCNQ^- nitrile stretching modes can be quantitatively described by using the framework of the vibrational Stark effect (VSE). There is a rich existing literature using the vibrational Stark shifts for a variety of nitrile, carbonyl, and other pendant groups to directly measure the local electric fields experienced in biological systems,[27−39] self-assembled monolayers,[40−44] solvated ion pairs,[45−48] and other applications.[49−51] Thus, by measuring the vibrational Stark shift of the nitrile stretches on the F_4TCNQ anion across a range of doped P3HT environments, we can directly infer the anion−hole separation distance. We also show that there is a direct correlation between the electric field experienced by the dopant anion and the degree of polaron coherence, allowing us to directly infer the degree of polaron delocalization. Overall, we demonstrate that the F_4TCNQ radical anion is more than just a dopant counterion, it also serves as a sensitive vibrational Stark probe, reporting directly on the strength of the local Coulombic interaction with polaronic charge carriers in doped P3HT.

2. EXPERIMENTAL METHODS

2.1. Materials. Electronic-grade poly(3-hexylthiophene-2,5-diyl) (P3HT) (4002-EE; 91−94% RR, M_w = 46−57 kg mol^{-1}, PDI = 2.3) was purchased from Rieke Metals. Sublimation grade F_4TCNQ (purity >98%) was purchased from TCI America. The synthesis, preparation, and characterization of the specially synthesized 100% RR P3HT have been described by us in prior work.[6] All materials and solvents were used as received without any further purification. Reusable KBr plates were used as substrates and first cleaned by polishing with a cotton swab soaked in chlorobenzene (CB). All subsequent fabrication steps described below were performed inside a N_2-filled glovebox.

2.2. Sequential Doping from CF/DCM Solvent Blends. For the polymer coating step, P3HT (20 mg mL^{-1}) in *o*-dichlorobenzene (ODCB) was spin-coated for 20 s at 1000 rpm to fully coat the substrate, while still keeping a thin layer of liquid ODCB dissolved P3HT intact. The wet films where then placed inside a Petri dish with the lid *off*, so that the solvent vapor could still collect inside the Petri dish volume but dissipate relatively quickly. This causes the solid polymer film to form over the course of 1−2 min. Subsequently, these pristine polymer films were solution doped with F_4TCNQ by spin-coating them using a doping solvent mixture of various ratios chloroform (CF) and dichloromethane (DCM) (F_4TCNQ concentration held at 1 mg mL^{-1}) at 4000 rpm for 10 s.

2.3. Fabrication of Pristine Polymer Films of Controlled Crystallinity and Sequential Doping. To tune the crystallinity of the pristine polymer films, we exploited solvent evaporation kinetics to control the drying time of the polymer layer. For the most disordered films, commercially available P3HT (10 mg mL^{-1}) was spin-coated out of chloroform (CF) (bp = 61.2 °C) for 60 s at 1000 rpm. To produce films with more order in the P3HT crystallites, the same commercially available P3HT (20 mg mL^{-1}) was spin-coated out of ODCB (bp = 180.19 °C) for 20 s at 1000 rpm. The still-wet films were then placed inside a *closed* Petri dish to prevent the solvent vapor from easily escaping, which extends the drying time to 3−4 h.

Finally, P3HT films with the most crystalline order were fabricated from an in-house synthesized batch of P3HT with virtually perfect regioregularity, confirmed via ^1H NMR.[6] Because of the high degree of regioregularity, the solutions were first heated to 60 °C to prevent aggregation and then spin-coated out of ODCB (20 mg mL^{-1}) for 20 s at 1160 rpm. The still-wet films were then placed inside a *closed* Petri dish to prolong the crystallization period.

3. MID-IR SPECTROSCOPY OF F_4TCNQ-DOPED P3HT FILMS

We have previously shown that sequential processing, casting the polymer film first and then infiltrating the dopant in a second solution- or gas-phase step, is a versatile technique capable of producing high-quality doped semiconducting polymer films.[6,12−14,52−55] This method also allows for tuning the degree of crystallinity in doped conjugated polymer films. For example, doped P3HT crystallinity can be tuned either by changing the processing conditions of the precast polymer film[6] or by careful choice of the solvent used in the subsequent doping step.[15]

Figure 1a shows a series of mid-IR absorption spectra for F_4TCNQ-doped P3HT films where the solvent used to introduce the dopant is composed of a mixture of chloroform (CF) and dichloromethane (DCM). By varying the blend ratio of these two solvents, we can exert a high degree of control over the resultant morphology. In previous work, we used grazing incidence wide-angle X-ray scattering (GIWAXS) to characterize the crystallinity of films produced this way and found that although the morphology and even the doping mechanism both become associated with increased amorphous regions as CF content increases in the doping solvent, the ordered regions that remain become more highly crystalline.[15] This is due to the strong dissolving power of the CF solvent, which allows for recrystallization of the ordered fractions of the precast P3HT film that remain following doping. Thus, the crystalline domains that do survive have a much higher average polaron coherence length than crystallites in films prepared with doping solvents where redissolution does not occur.[15]

The crystallinity of F_4TCNQ-doped P3HT films also can be manipulated during the initial polymer spin-coating step, as shown in Figure 1b. In this case, we exploit both the polymer regioregularity and the polymer casting solvent drying kinetics to control the polymer order. We previously have used GIWAXS to show that when a commercial P3HT film is cast from CF, a fast-drying solvent, the resultant polymer film is highly amorphous with relatively little crystallinity.[6] In contrast, when commercially available P3HT is cast from the more slowly drying solvent *o*-dichlorobenzene (ODCB), the films have more time to order and become more crystalline. Finally, by using a specially synthesized batch of P3HT with virtually 100% regioregularity,[6,56] also cast from ODCB, we can obtain highly crystalline P3HT films (see the Supporting Information for experimental details). We also showed that when the film crystallinity is tuned this way, the crystalline regions of the polymer dope first, and the amorphous regions only become doped at very high doping concentrations after the crystalline regions are filled.[6]

3.1. Spectral Signatures of P3HT Polaron Coherence Following Doping with F_4TCNQ. Spano and co-workers have developed a theory for doped conjugated polymers that describes how changes in the energetic and structural disorder of a polymer affect polaron coherence, that is, the degree to which the polaron is delocalized along the P3HT backbone and/or between adjacent π-stacked P3HT chains.[6−10] The theory indicates that as the polaron coherence changes, there is a corresponding shift in both the position and shape of the mid-IR polaron electronic absorption spectrum. In this model, one of the primary features that affects the polaron coherence length is the strength of the Coulombic interaction between the positively charged, delocalized hole on the polymer and the corresponding countercharge located on the dopant molecule. The model can reproduce experiment remarkably well for a variety of conjugated polymer−dopant pairs.[6−10]

In the present work, the most crystalline of the F_4TCNQ-doped P3HT samples (Figure 1 purple curve in panel a and

https://doi.org/10.1021/acs.chemmater.1c02934
Chem. Mater. XXXX, XXX, XXX−XXX

light green curve in panel b) show the characteristic P3HT polaron absorption from highly ordered environments. Because the hole is better able to delocalize in such environments, there is less Coulombic attraction between the hole on the polymer and dopant counterion, as discussed further in section 3.1. This weakened Coulombic interaction and larger coherence lengths are manifest spectroscopically by both increased relative absorption intensity for peak "A" (the rough feature centered near ~0.16 eV), and a shift to lower energies for peak "B" (the main, smoother feature whose maximum falls between 0.35 and 0.55 eV depending on the sample).

In contrast, the curves in maroon (panel a) and blue (panel b), which are for the most disordered doped P3HT films, show mid-IR absorption spectra characterized by a relatively low absorption intensity of the A peak and a shift of the B peak to higher energies. This is a hallmark of poor polaron coherence.[7−10] Because the amplitude of peak A decreases relative to peak B with increasing hole localization, the amplitude ratio of peaks A/B becomes a simple metric for tracking changes in polaron delocalization in doped conjugated polymers.[7−10]

For the method of controlling morphology by adjusting the doping solvent (panel a), the A/B ratio increases from A/B = 0.55 when casting F_4TCNQ from pure DCM, up to A/B = 0.81 when casting the dopant from pure CF. When altering the morphology during the polymer casting step (panel b), the change in the A/B ratio is nearly identical, with A/B = 0.56 when the polymer is cast from CF and A/B = 0.81 for slow-dried films fabricated from 100% regioregular P3HT. Because of the relatively small physical size of the F_4TCNQ anion, the Coulombic interaction between the anion and the hole polaron has enough strength that increasing the local order of the polymer can only tune the degree of polaron delocalization over a somewhat limited range compared to what is achievable with larger dopants designed to minimize the polaron−dopant Coulombic interaction.[13,14]

The theory developed by Spano and co-workers provides a direct connection between polaron coherence lengths and spectral A/B ratios.[9] In this work, we experimentally measure the change in polaron coherence length by estimating the strength of the electric field between the F_4TCNQ^- counterion and the hole polaron on P3HT. Our approach is possible because the theoretical relationship between the A/B spectral ratio and polaron coherence is predicted to be roughly linear across a wide range of coherence length values.[9] For our doped P3HT films with different degrees of order, the measured A/B ratios range from ~0.55 to 0.81, which should correspond to an ~25% change in the average polaron coherence length.[9] In the sections that follow, we will show how shifts in the energy of the F_4TCNQ vibrational modes allow us to map out the local electrical fields in doped P3HT films to precisely determine the change in polaron coherence length.

3.2. F_4TCNQ^- Nitrile Vibrational Spectrum in Doped P3HT Films. F_4TCNQ^- has two IR-active vibrational modes with significant oscillator strength in the so-called transparent window between 1800 and 2500 cm^{-1}: these are C≡N stretching modes with B_{1u} and B_{2u} symmetry, illustrated in Figure 2a, which in doped P3HT films occur near 2190 and 2170 cm^{-1}, respectively. An example IR spectrum of F_4TCNQ-doped P3HT produced by sequential processing is shown in Figure 2b. Meneghetti and Pecile have noted that the location and geometry of the nitrile substituents on this molecule make

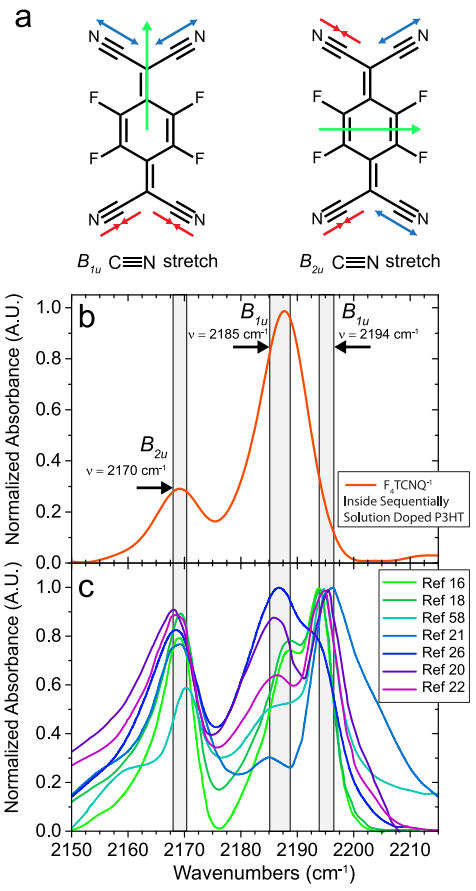

Figure 2. (a) Atomic displacement vectors for the two F_4TCNQ C≡N vibrational modes with B_{1u} and B_{2u} symmetry. Compression and expansion of the C≡N bonds is indicated red and blue arrows, respectively. The difference dipoles (green arrows) for these two modes point along the long axis of the molecule for the B_{1u} mode and across the short molecular axis for the B_{2u} mode. (b) FTIR spectrum of the F_4TCNQ^- radical anion inside sequentially solution-doped P3HT (with the dopant cast from 1 mg mL^{-1} *n*-butyl acetate) and (c) inside blend-doped P3HT samples taken from various literature references, in descending order on the legend: Pingel et al. (ref 16), Ghani et al. (ref 18), Mendez et al. (ref 58), Jacobs et al. (ref 21), Hase et al. (ref 26), Neelamraju et al. (ref 20), and Watts et al. (ref 22).

these two vibrational modes uniquely susceptible to their local environment.[57] In fact, this susceptibility to local environment should make these modes relatively poor indicators for quantitatively measuring the degree of charge transfer, a subject of much recent interest.[15,17−25]

The literature on the vibrational spectroscopy of the F_4TCNQ radical anion inside films of doped P3HT shows that the two nitrile stretches can absorb at a variety of locations.[16,18,20−22,26,58] In Figure 2c, we have reproduced the IR spectra of F_4TCNQ^- in doped P3HT films taken from seven different recent sources in the literature; it is clear that different groups observe different F_4TCNQ anion vibrational spectra for what is nominally the same doped polymer system.

All of the data shown in Figure 2c were taken on films prepared by blend doping, where the polymer and dopant were mixed together in solution prior to casting. This method has the advantage of providing a precise dopant-to-monomer ratio but suffers from several drawbacks, including yielding a very poor film morphology.[6,52,53] We can see that for blend casting

https://doi.org/10.1021/acs.chemmater.1c02934
Chem. Mater. XXXX, XXX, XXX−XXX

the B_{1u} and B_{2u} modes usually appear near 2194 and 2170 cm^{-1}, respectively. However, the spectra in Figure 2c show an additional vibrational peak between these two modes, centered near 2185 cm^{-1}. The specific origin of this peak has been a topic of debate.[16,18,20−22,58] In early work, this 2185 cm^{-1} peak was tentatively assigned to a C≡N stretching mode of A_g symmetry,[16,17] which would require a break in planarity of the F_4TCNQ anion. Such a nonplanar geometry might occur if F_4TCNQ-doped P3HT in a π-stacking arrangement.[59] The more recent consensus, however, is that F_4TCNQ^- resides in the lamellar side-chain regions of the doped P3HT crystallites,[6,11,12,24,26,53,60−65] so that the 2185 cm^{-1} mode must result from some other phenomenon.[22]

One important clue to the assignment of the 2185 cm^{-1} peak comes from Hase et al.,[26] who showed that upon exposing F_4TCNQ-doped P3HT films to extended thermal annealing cycles, the B_{1u} absorption feature near 2194 cm^{-1} becomes reduced in amplitude, leaving behind the peak near 2185 cm^{-1} and the B_{2u} mode near 2170 cm^{-1}. Watts et al. subsequently noted that if the unknown peak near 2185 cm^{-1} did belong to an A_g mode, then the two features near 2185 and 2194 cm^{-1} should show similar behavior upon annealing.[22] The fact that annealing causes a loss in amplitude only for the 2194 cm^{-1} mode suggests that this vibrational feature is associated with a local structure that can change upon annealing. Thus, it seems far more likely that the two features near 2185 and 2194 cm^{-1} both belong to the B_{1u} mode, where the specific vibrational energies are reporting something about variations in the local environment.

With the idea that the F_4TCNQ^- nitrile stretching modes shift with their local environment, we now examine how the doped film processing method, which controls P3HT crystallinity and polaron delocalization, affects the resulting dopant nitrile vibrational spectrum. Figure 2b shows the intensity-normalized nitrile vibrational spectrum of the F_4TCNQ radical anion inside sequentially doped P3HT using the relatively noninteracting solvent *n*-butyl acetate to infiltrate the dopant at a concentration of 1 mg mL^{-1}. It is clear from comparing panels b and c in Figure 2 that the dopant anion vibrational spectrum for sequentially doped films is considerably different from those obtained from blend doping. Rather than seeing two peaks for the B_{1u} mode distributed between 2194 and 2185 cm^{-1}, the sequentially doped film shows only a single feature centered at 2187 cm^{-1}. This suggests that for sequential processing, which generally produces more ordered doped P3HT films, the dopant molecules have a singular well-defined geometry in the polymer crystallites. The higher-energy B_{1u} peak near 2194 cm^{-1}, in contrast, must belong to anions that Coulombically trap the hole in the morphologically disordered polymer regions that predominate in blend-cast doped films.

3.3. Correlation between Polaron Coherence and F_4TCNQ^- Vibrational Spectrum. Now that we have established a basis for understanding how the doped polymer structural environment should affect the vibrational spectrum of F_4TCNQ^-, we can consider precisely how the local degree of order and polaron coherence affect the nitrile stretching frequencies. Figure 1c shows the vibrational spectrum of the F_4TCNQ radical anion inside P3HT films sequentially doped with F_4TCNQ cast from CF/DCM solvent blends. We see that when the dopant is infiltrated from pure CF, the principal B_{1u} nitrile absorption feature occurs with ν_{max} = 2185 cm^{-1} (purple curve). As the polaron becomes increasingly localized by increasing the fraction of DCM in the doping solvent, the B_{1u} vibrational peak monotonically shifts to ν_{max} = 2189 cm^{-1} (maroon curve). It is worth noting that even in these high-DCM processed P3HT films, which are the most disordered made by sequential doping, the B_{1u} mode is still five wavenumbers lower in energy than the 2194 cm^{-1} peak seen in the even more disordered blend-doped P3HT films.

When we analyze the principal vibrational features in the sequentially doped films seen in Figure 1c in more detail, we see that they are actually best fit to two Gaussians: a dominant feature that shifts between 2188 and 2185 cm^{-1} (shaded purple curve reduced to 0.3 intensity) and a smaller shoulder (shaded maroon curve) located near 2194 cm^{-1} (see the Supporting Information for fitting details). As the polarons in the crystalline regions become more delocalized by increasing the fraction of CF, the intensity of this small peak shoulder near 2194 cm^{-1} monotonically decreases and disappears entirely when the dopant is cast from 100% CF. The fact that the peak near 2194 cm^{-1} decreases with a higher fraction of CF solvent and thus increasing local crystalline order fits well with the notion that this higher energy peak is associated with highly localized polarons, which are more likely to exist in more disordered polymer regions. This also helps to explain why the peak near 2194 cm^{-1} presents so prominently in films produced by blend doping, since blend-cast films are expected to have a broader distribution of morphological states.

A similar trend for the F_4TCNQ^- B_{1u} vibrational mode also occurs when the doped polymer crystallinity is tuned by changing the how the polymer film is cast (with the dopant solvent held constant), as shown in Figure 1d. When the underlying P3HT film is 100% regioregular and cast from ODCB, the F_4TCNQ^- B_{1u} mode has ν_{max} = 2186 cm^{-1}. As the polaron becomes more localized when the initial P3HT film is cast from CF, we see the B_{1u} mode shift up to ν_{max} = 2191 cm^{-1}.

For both sets of doped P3HT films, we see a remarkably strong correlation between the P3HT polaron coherence, as measured by the A/B spectral intensity ratio, and the position of the F_4TCNQ^- B_{1u} nitrile stretch, as summarized in Figure 1e. This correlation is one of the principal results of this work: the position of the B_{1u} stretching peak of the dopant provides a local measure of polaron coherence on the polymer. The F_4TCNQ^- B_{1u} nitrile stretching spectra seen in Figure 2c behave in a fundamentally predictable way if the degree of polaron coherence is known. Thus, the variations measured by different groups directly reflect differences in polaron coherence resulting from different methods of fabricating the doped films.

As an aside, we note that in both sets of doped P3HT films studied in Figure 1, we see an increased amplitude for the F_4TCNQ CTC vibrational peak near 2200 cm^{-1} with increasing polymer disorder.[15] The reason the CTC peak becomes more prominent when the doping solvent has an increasing fraction of CF is because the use of CF as a sequential doping solvent causes significant disruption of the P3HT crystal lattice. This is what both increases the total fraction of disordered regions and also increases the order of the crystalline regions that remain.[15] When using more common and milder processing solvents, however, it is clear that CTC formation is mostly limited by the relative amount of disordered polymer regions.

For the subset of our F_4TCNQ-doped P3HT samples where the F_4TCNQ^- B_{2u} mode did not have a neighboring low-

https://doi.org/10.1021/acs.chemmater.1c02934
Chem. Mater. XXXX, XXX, XXX−XXX

energy shoulder (which has been previously attributed to the B_{3g} mode near ν = 2160 cm^{-1},[18,66] or simply remained an unassigned mode[20,22]), we can cleanly fit both the position and width of the B_{2u} peak. We find that the vibrational energy of this mode does not shift in different P3HT environments, always remaining within a 2 cm^{-1} range. However, we do see that the full width at half-maximum (FWHM) of the F_4TCNQ^- B_{2u} feature broadens from 8.1 cm^{-1} for doped P3HT films with the most localized polarons (lowest A/B ratio) up to 12.5 cm^{-1} for doped films with the most delocalized polarons (highest A/B ratio), a correlation summarized in Figure 1f. The fact that the peak width of the B_{2u} mode correlates with polaron coherence, not the peak vibrational energy, provides another crucial piece of information that will allow us to quantify both the orientation of the F_4TCNQ anion relative to the P3HT polaron and the degree of polaron delocalization.

Although the two series of doped P3HT films we have studied in Figure 1 modify the local polymer crystalline order during different processing steps, they show a similar range of polaron coherence, as evidenced by the A/B spectral ratio, and a similar behavior of the B_{1u} and B_{2u} vibrational modes, summarized in Figures 1e and 1f. For the most locally ordered P3HT films from each set (100% RR precast P3HT film and commercial P3HT with the dopant cast from 100% CF), the mid-IR spectra have an identical A/B ratio of 0.81 and correspondingly similar B_{1u} vibrational peak positions of 2185−2186 cm^{-1} as well as similarly broad B_{2u} vibrational peak widths of ∼12.2−12.5 cm^{-1}. This represents the highest A/B ratio, smallest B_{1u} vibrational frequency, and broadest B_{2u} peak width that we have observed for this polymer−dopant combination. Thus, it is likely these values are approaching the fundamental upper limit for polaron delocalization when F_4TCNQ is used to dope highly ordered P3HT.

Why would there be a fundamental upper limit to polaron delocalization? We expect polaron delocalization to be determined by two primary factors: (i) the inherent energetic disorder due to structural imperfections in the polymer crystallites and (ii) the strength of the Coulombic interaction between the hole and dopant counteranion.[7−10] Because the dopant preferentially occupies crystalline regions of P3HT films,[6,53] the distance between the anion and the polymer backbone, d_{anion}, depends mainly on the physical size of the anion.[13,14] For the doped P3HT samples whose properties are shown in Figure 1, d_{anion} is essentially fixed, so the increases we see in polaron coherence and the corresponding changes in the vibrational modes must result from increases in the local structural order of the polymer.

All of this means that the extent of polaron delocalization in the most-ordered polymer regions is limited by the minimum possible strength for the hole−counterion Coulombic interaction. F_4TCNQ-doped P3HT has a lamellar spacing of ∼17 Å,[6,15] so the maximum possible dopant−polaron distance is ∼7−8 Å. Because of this relatively short distance, the Coulombic interaction from F_4TCNQ^- always causes some localization of the polaron beyond what is intrinsically allowed by a highly ordered polymer structure.[6,9] This explains why the F_4TCNQ-doped P3HT system has a relatively limited doping efficiency and carrier delocalization[67] and why the use of physically larger dopants that screen the Coulombic interaction can produce polarons with even greater delocalization in P3HT (A/B ratios greater than unity).[13,14] The idea that dopant anions can only reside in a limited set of places also helps to explain why F_4TCNQ-doped P3HT films always display some absorption of the most weakly shifted B_{1u} nitrile peak near 2185 cm^{-1}: even in blend-cast films with a relatively poor overall morphology, there are always a few doped P3HT crystallites with a reasonable degree of order.

The strength of the Coulombic interactions between the polaronic charge carriers and their dopant counterions is also expected to impact the measured electrical conductivity of doped conjugated polymer films. In theory, smaller Stark shifts indicate lower Coulombic binding between the polaron and counterion, which should result in higher electrical conductivity. For the series of samples where the polymer crystallinity is controlled in the polymer casting step, this is precisely what we see, as shown in Table S9. However, for the series of samples where the doping solvent properties were altered, a significant number of F_4TCNQ dopants begin to dope via CTC formation. CTC doping results in carriers that are several orders of magnitude less mobile than those created by ICT doping, so the presence of a significant number of CTCs leads to a decrease in conductivity despite the diminished Stark shift of the counterions in the crystalline regions. We have explored the nature of the CTC doping in samples like these and the effects on charge transport characteristics in previous work.[15]

4. F_4TCNQ AND THE VIBRATIONAL STARK EFFECT

Now that we have established a clear correlation between the behavior of the C≡N vibrational stretches of F_4TCNQ^- and the degree of polaron coherence in doped P3HT films, we can turn our attention to considering the mechanisms that cause these changes to take place.

The central thesis of this paper is that the blue-shift of the B_{1u} mode and broadening of the B_{2u} mode with increasing A/B ratio occur as a direct result of the vibrational Stark effect (VSE). The VSE arises from the interaction between a molecule's vibrational mode and an externally applied electric field. If vibrational excitation of a particular mode changes the dipole of the molecule, then the difference dipole vector between the ground and excited vibrational states can interact with the aligned component of an external electric field, causing a shift in the resonant energy for that vibrational mode. Because external fields are usually weak relative to the internal fields that hold a molecule together, the VSE can be well described by first-order perturbation theory, and the shift of the vibrational frequency is roughly linear with the local field strength.

The VSE is well studied in the literature, and its primary use has been to understand the electric fields present in biological systems.[27−39] The VSE also has been recently used to directly study ionic interactions in solution, allowing researchers to determine if dissolved salts exist as contact ion pairs, solvent-separated ion pairs, or truly free solvated ions.[45−47] In many applications, VSE probes are simple alkylnitrile substituents, for which the difference dipole is aligned along the internuclear axis of the C≡N triple bond. The F_4TCNQ anion, in contrast, has two pairs of nitrile groups. Figure 2a shows the atomic displacement vectors for the F_4TCNQ^- B_{1u} and B_{2u} nitrile stretching modes with bond compression indicated in red, bond expansion in blue, and the difference dipole vectors in green. The difference dipole vector for the B_{1u} mode points along the long axis of the molecule, while that of the B_{2u} mode points transversely across the short axis. So although F_4TCNQ was not specifically designed for this purpose, it is clear that

https://doi.org/10.1021/acs.chemmater.1c02934
Chem. Mater. XXXX, XXX, XXX−XXX

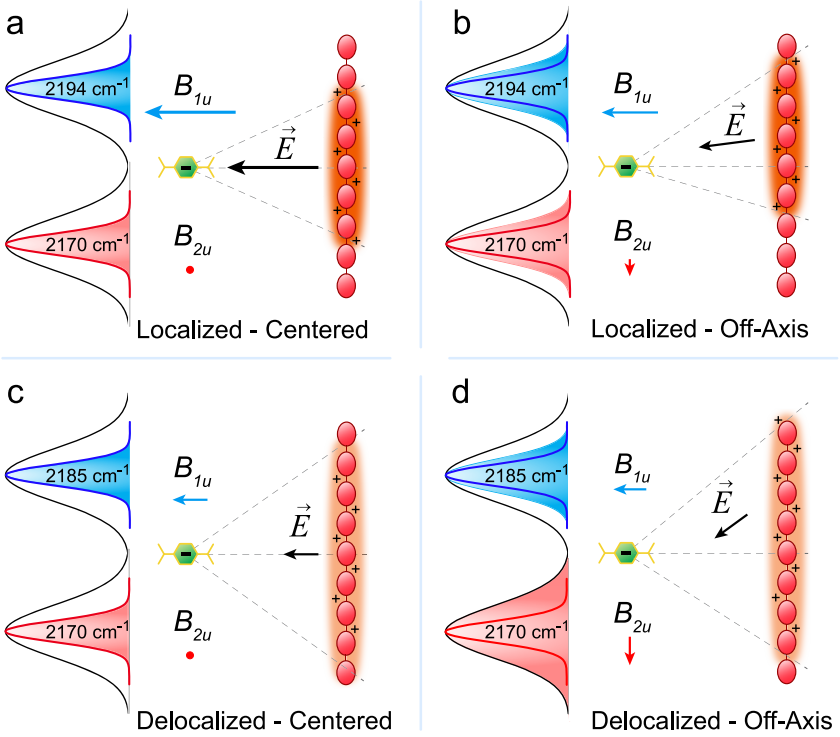

Figure 3. Cartoons illustrating how the electric field from a variety of polaron geometries influences the vibrations of the F_4TCNQ anion. (a) A localized P3HT polaron centered along the dopant−polymer axis produces a strong electric field aligned with the F_4TCNQ^- B_{1u} difference dipole, resulting in a VSE shift to a higher vibrational energy. The centered geometry has no electric field component aligned along the B_{2u} difference dipole, so there is no VSE shift of that mode. (b) A localized P3HT polaron with a slightly off-axis geometry slightly lowers the electric field component experienced by the B_{1u} vibration and slightly increases that experienced by the B_{2u} vibration, leading to a slight broadening of both modes. (c) A more delocalized P3HT polaron centered along the dopant−polymer axis exerts a lower field strength on the F_4TCNQ anion than the localized polaron case in panel a, resulting in a smaller VSE shift of the B_{1u} mode, which appears at a lower vibrational energy. (d) A more delocalized P3HT polaron with an off-axis geometry has little effect on the B_{1u} mode, but the increased electric field component along the B_{2u} mode leads to an increase in VSE broadening.

this dopant molecule contains all of the essential machinery required to operate as a vibrational Stark probe.

4.1. Coulombic Interactions and the Vibrational Stark Effect in F_4TCNQ-Doped P3HT Films. The fact that the difference dipoles of the B_{1u} and B_{2u} modes point in perpendicular directions allows us to directly infer the orientation of the dopant anion relative to the polaron on the polymer backbone that generates the local electric field. As mentioned above, X-ray diffraction work from several groups has determined that F_4TCNQ^- sits in the lamellar side-chain regions of the P3HT crystallites.[6,11,12,24,26,53,60,61,63,64] In addition, Brinkmann and co-workers, who studied rub-aligned F_4TCNQ-doped P3HT films by using polarized absorption spectroscopy, have shown that the long axis of the F_4TCNQ^- anion sits perpendicular to the polymer backbone.[62,65,68−70] This means that the difference dipole vector of the B_{1u} mode is oriented parallel to the electric field lines emanating from the hole on the polymer backbone (Figure 3), while that of the B_{2u} mode lies perpendicular to the local field.

Figures 3a,c illustrate how the VSE shifts the resonant energy of the F_4TCNQ^- B_{1u} mode in direct response to changes in the magnitude of the P3HT hole-generated electric field. At fixed d_{anion}, the strength of the field will decrease as the polaron becomes increasingly delocalized. This provides a simple explanation as to why the frequency of the F_4TCNQ^- B_{1u} mode, whose difference dipole is oriented parallel with the field lines from the polaron, exhibits a strong vibrational Stark shift in response to changes in polaron coherence length (i.e., with A/B spectral ratio, as seen in Figure 1e).

In contrast, the peak vibrational energy of the F_4TCNQ^- B_{2u} mode does not change with polaron coherence length; it only broadens. This is because the orientation of the B_{2u} mode difference dipole is mostly orthogonal to the hole-generated electric field. This means that any Coulombic interaction between the polaron and the difference dipole of this mode must originate from an off-axis electric field component. In the simplest case where the polaron is centered on the polymer-dopant axis (Figures 3a,c), there is no net off-axis field component that might be aligned with the B_{2u} mode, explaining why this peak does not shift in response to changes in polaron coherence.

However, there is no guarantee that a polaron will always be centered along the dopant−polaron axis; in fact, we expect some degree of along-the-chain disorder of the dopant location relative to the polaron position in F_4TCNQ-doped P3HT films. This means that the magnitude of the polaron E_{field} component aligned with the B_{2u} difference dipole will increase not only with the amount of off-center displacement but also with the degree of polaron delocalization, as illustrated in Figures 3b,d. If the total lateral disorder is modest, the result will be a net broadening of the B_{2u} mode rather than a shift, exactly as observed in Figure 1f. This is because, on average, the polaron is still centered relative to the location of the anion, so the off-axis component is relatively weak compared to

https://doi.org/10.1021/acs.chemmater.1c02934
Chem. Mater. XXXX, XXX, XXX−XXX

the field strengths experienced along the B_{1u} difference dipole direction.

It makes sense that there should be a relatively strong correlation between the width of the F_4TCNQ^- B_{2u} nitrile stretch and the degree of polaron delocalization, but it is also possible that broadening of the B_{2u} mode might occur if the dopant anions had significant orientational disorder relative to the direction of the electric field from the polaron. If there were orientational disorder, however, the B_{2u} peak would be expected to narrow as the degree of local polymer crystalline order increased. Instead, we observe the opposite: the B_{2u} peak broadens as the polymer film becomes more ordered. This verifies that the observed correlation of the anion vibrational spectrum with the delocalization of the polaron indeed comes from the most ordered regions in the doped films and is not representative of orientationally disordered areas of the film.

Finally, it is conceivable that at sufficiently high doping levels a second polaron on a neighboring chain could exert a field on the F_4TCNQ molecule that would work to counteract the field from the first polaron, reducing the observed Stark shift. However, Figure S13a shows that the magnitude of the Stark shift does not change over a wide range of doping concentrations. This confirms that the doping levels we used to analyze the Stark shifts in this work are not high enough to encounter this effect, though it might be observed at higher dopant to monomer ratios.

4.2. Stark Tuning Rate: Estimating Local Electric Field Strengths with Vibrational Mode Shifts. The above evidence strongly indicates that the VSE can explain all of the observed changes in the F_4TCNQ^- nitrile vibrations as resulting from changes in polaron delocalization in doped P3HT films. In the next sections, we work to quantify the strength of these interactions to experimentally extract the anion−hole distance and degree of polaron delocalization.

It is well established that there is a linear relationship between the shift of a vibrational mode and the strength of the applied field. The magnitude of the vibrational shift per unit applied field is known as the Stark tuning rate (STR) parameter. To the best of our knowledge, the STR parameters have only been experimentally measured for a very limited number of conjugated molecules. For Stark probe molecules with multiple nitrile groups, similar to F_4TCNQ, the STRs tend to fall within the range of 1−3 $cm^{-1}/(MV\ cm^{-1})$. This is considerably higher than the STR's of isolated nitrile groups, which typically are a factor of 2 smaller.[31,32,42] Suydam and Boxer experimentally measured the STRs for a variety of mono- and disubstituted nitrile containing conjugated molecules.[30] These workers reported a STR of 2.9 $cm^{-1}/(MV\ cm^{-1})$ for the B_{2u} mode and 1.4 $cm^{-1}/(MV\ cm^{-1})$ for the B_{1u} mode of a dicyanomethylene−polyene compound of similar size to F_4TCNQ. We will assume that these values also describe the Stark effect of the F_4TCNQ vibrational modes, allowing us to quantitatively explore the relationship between the measured linear stark shift and the change in the polaron delocalization length, as measured via the polymer mid-IR absorbance spectrum. We discuss our theoretical efforts to calculate the STR parameters of the F_4TCNQ anion, and why they fail at the DFT level of theory, in the Supporting Information.

4.3. Using the VSE to Directly Measure Polaron Delocalization in F_4TCNQ-Doped P3HT Films. With this estimation of the Stark tuning rate parameters in hand, we now use these values, along with the data presented in Figure 1, to determine how the polaron coherence length changes across the experimentally observed range of A/B values. We begin by considering the predicted magnitudes of the fields experienced by the B_{1u} and B_{2u} modes as a function of polaron delocalization and the anion−hole separation distance, d_{anion}. For this calculation, we consider the field experienced by the anion at a single point located at d_{anion} away from the center of the P3HT chain. We then approximate polaron delocalization as resulting from a single positive charge spread out uniformly along a one-dimensional line of length L, given in units of the number of P3HT monomers. We then model changes in polaron coherence as L increases from 1 to 9 (Figure 4a), so that the one-dimensional polaronic charge density goes as $1/L$. Our model assumes a dielectric constant of unity, as the short-range interactions between the polaron and anion likely do not experience the dielectric value of the bulk material—an assumption which is consistent with what others have chosen

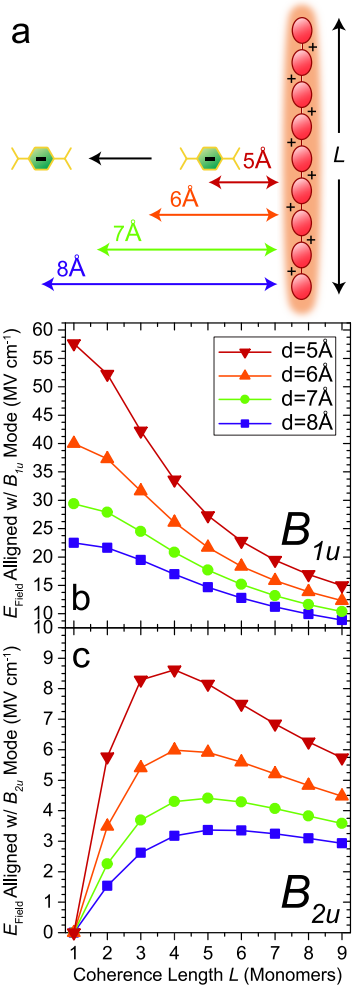

Figure 4. (a) Cartoon of hole polaron delocalization along the P3HT backbone, modeled as a line of uniform charge density q^+/L, where q^+ is the elementary charge and L is the delocalization length. (b) Electric field component experienced by the F_4TCNQ anion B_{1u} mode from the line of charge is calculated as a function of delocalization from a single monomer up to a length of 9 monomer units for a range of anion distances from 5 up to 8 Å. (c) Electric field component from half of the delocalized polaron, chosen as a proxy to represent along-the-chain disorder, along the F_4TCNQ B_{2u} difference dipole. The magnitude of this component is an order of magnitude smaller than that along the B_{1u} direction.

https://doi.org/10.1021/acs.chemmater.1c02934
Chem. Mater. XXXX, XXX, XXX−XXX

for similar inquiries.[6,7,9] We note that our model ignores interchain polaron coherence—a choice made because work from Ghosh and co-workers predicts that the way in which the coherence length changes with the spectral A/B ratio is roughly the same regardless of whether the delocalization is spread over one chain or between multiple chains.[9] Because of this, we do not expect delocalization between neighboring chains to significantly affect the electric fields experienced by a nearby F_4TCNQ anion. Finally, even though we expect some along-the-chain disorder, we assume that, on average, the anion is centered along the length of the delocalized polaron.

The main difficulty associated with quantitatively determining the change in P3HT polaron coherence length from the VSE of the F_4TCNQ nitrile stretching modes is that we only have access to the experimentally measured vibrational shifts that occur within a range of externally applied fields: we do not know the absolute magnitudes of these fields because we do not know the position of the B_{1u} stretching mode inside a P3HT film in the absence of any external fields. Thus, the best we can do is to use the measured shift in the B_{1u} peak vibrational energy, along with the STR, to determine the change in electric field associated with the ∼25% increase in polaron coherence length measured by the spectral A/B ratio in Figure 1. Once we have calculated the change in electric field experienced by the B_{1u} mode, we can then use the measured change in width of the B_{2u} mode, which experiences a field from the same delocalized polaron, to experimentally determine both the value of d_{anion} and the physical polaron coherence length increase that can explain the vibrational Stark features of both modes.

Figure 4b shows how the strength of the electric field aligned with the B_{1u} difference dipole is affected as polaron delocalization is increased from 1 to 9 monomer units. As argued above, the maximum possible dopant−polaron distance in a P3HT crystallite is half the lamellar spacing, or only ∼7−8 Å.[6,15] Thus, by examining a range of possible anion−hole distances up to 8 Å, we can narrow down the possible range of fields exerted by a P3HT polaron on the nitrile stretching modes of F_4TCNQ^-. In Figure 4b, the dark blue squares corresponding to d_{anion} = 8 Å show that increasing the degree of polaron delocalization diminishes the strength of the electric field experienced by the anion to ∼39% of its original value. Because this is the largest possible anion−hole distance, it also represents the minimum possible decrease in the relative field strength for a 1 to 9 unit change in polaron delocalization. For shorter anion−hole distances, such as d_{anion} = 5 Å (red triangles), the relative electric field strength drops to ∼26% of its starting value as the polaron delocalizes from 1 to 9 monomer units. We do not expect more sophisticated models to deviate significantly from these trends, since fundamentally this is an interaction described by Coulomb's law.

For the B_{2u} mode, our simplified model does not predict any net electric field alignment with the difference dipole. However, we can approximate the effects of along-the-chain disorder (cf. Figures 3b and 3d) by considering the field contribution from just half of the delocalized polaron along the positive axis. Figure 4c shows the magnitude of the electric field component from half of the delocalized charge that is aligned parallel with the B_{2u} mode as a function of both polaron coherence length and d_{anion}. In this case, we see that the electric field does not vary monotonically with polaron delocalization because of competing effects. At shorter polaron coherence lengths, additional delocalization creates additional off-axis field alignment, which raises the overall magnitude of the field component along the B_{2u} difference dipole. However, at longer coherence lengths, additional delocalization lowers the line charge density, which contributes to a net reduction in the total magnitude of the field.

In our simple model, the predicted magnitudes of the fields experienced by the F_4TCNQ^- B_{2u} mode are nearly an order of magnitude lower compared to those experienced by the B_{1u} mode. This is indeed consistent with the fact that the B_{2u} mode only slightly broadens and does not shift with changing P3HT polaron delocalization, as measured by the A/B spectral ratio, while the B_{1u} mode shows a definite Stark shift as polaron coherence changes with the local polymer order.

As mentioned above, theoretical work based on Spano's model[9] indicates that our range of measured A/B ratios corresponds to an ∼25% increase in P3HT polaron coherence length; this change of coherence is the same whether or not the delocalization is along or between the polymer chains. With an estimated B_{2u} STR of ∼2.9 $cm^{-1}/(MV\ cm^{-1})$ and the observed (single edge) vibrational peak broadening of 2.2 cm^{-1}, the observed 25% change in polaron delocalization corresponds to a change in electric field of 0.76 MV cm^{-1}. Note that because the E_{field} alignment does not change monotonically for this mode, we cannot determine the sign of this change or the distance from which the delocalized polaron exerts the field.

However, the same delocalized polaron electric fields that change the width of the B_{2u} mode also cause the Stark shift of B_{1u} mode. Pairing our estimated STR parameter for the B_{1u} mode as ∼1.2 $cm^{-1}/(MV\ cm^{-1})$ with the experimentally measured vibrational shift of 5.79 cm^{-1}, the electric field experienced by this mode decreases by 4.9 MV cm^{-1} over this range of A/B ratios. Figures 4b,c show that the only way for F_4TCNQ^- to experience both of these field components for an ∼25% change in polaron coherence at a single distance is when the intrachain coherence length increases from 6 to 7.5 monomer units with an anion−hole separation distance of ∼6 Å. A set of tables summarizing the possible changes in field strength for different coherence lengths and separation distances can be found in the Supporting Information. Thus, by use of the VSE, it is possible to experimentally link the spectral A/B ratio to a specific degree of intrachain polaron delocalization.

Rather than assuming the ∼25% change in delocalization length from theory, we can also do the same analysis by first assuming a fixed ∼6 Å distance for d_{anion} based on X-ray diffraction.[6] The measured field-induced changes of the two F_4TCNQ^- modes are then only consistent with a coherence length change of ∼25% from 6 to 7.5 monomer units, so that no matter what our starting assumptions, there is only a single internally consistent value for the experimentally determined intrachain polaron coherence lengths.

Thus, by using the two orthogonally oriented nitrile vibrational modes of F_4TCNQ^- as independent measurements of the electric field, we can build a comprehensive picture of the charge carrier−dopant interactions in F_4TCNQ-doped P3HT films. The experimentally determined change in intrachain polaron coherence length from 6 to7.5 monomer units is consistent with what has been put forward previously for this system.[7] The Stark-determined d_{anion} of 6 Å also fits well with the X-ray scattering determined lamellar stacking distances[6,15] (see Table S3) as well as previously modeled anion distances based on the profile shape of the mid-IR polaron absorbance of F_4TCNQ-doped P3HT system.[6,7,9]

https://doi.org/10.1021/acs.chemmater.1c02934
Chem. Mater. XXXX, XXX, XXX−XXX

5. CONCLUSIONS

In summary, we have shown that the nitrile stretches of the commonly used dopant F_4TCNQ make an exquisite vibrational Stark probe of the local electric fields in doped conjugated polymer films, allowing us to uncover detailed information about P3HT polaron coherence. The fact that we observe one mode shift with polaron coherence while the other only broadens directly demonstrates that the dopant anion has a preferred orientation with respect to the polymer backbone. This is consistent with the idea that dopants prefer to reside in the lamellar regions of polymer crystallites, reinforcing conclusions in the literature reached by X-ray scattering[6,11,12,24,26,53,60,61,63,64] and by polarized spectroscopy of rub-aligned films.[62,65,68−70]

More importantly, we have provided the first experimental evidence that shows it is the degree of polaron delocalization that is directly responsible for the commonly seen changes in the F_4TCNQ^- nitrile vibrational spectrum in doped P3HT films with varying degrees of crystalline order. This verifies theories that argue the polaron A/B spectral ratio (and position of the B polaron absorption band) are indeed direct experimental signatures of polaron coherence. With a simple model, we can use the magnitudes of the observed vibrational spectral shifts and broadening to pin down precisely how the local electric field changes with polaron delocalization in different P3HT environments. The field magnitudes experimentally prove that the anion−polaron distance in F_4TCNQ-doped P3HT films is ∼6 Å and that intrachain polaron coherence lengths of roughly 6−7.5 monomer repeat units can be produced by varying the degree of local order through the film processing conditions.

Our results also allow us to explain the previous uncertainty over how to assign the vibrational spectrum of F_4TCNQ^- in doped P3HT films. The various vibrational lines that have been observed occur as a direct result of the unique preparation conditions and dopant/polymer blend ratios which produce a range of structural morphologies and polaron delocalization lengths. This in turn causes the dopant anions to experience a range of local electric fields, ultimately shifting the resonant vibrational energies. This also means that using the positions of the F_4TCNQ anion nitrile vibrations to determine the precise degree of charge transfer in charge-transfer complexes, usually associated with a feature near 2200 cm^{-1}, is potentially fraught with difficulty as electric fields from nearby integer charge-transferred polarons may also be responsible for shifts of this mode.

For the F_4TCNQ−P3HT materials combination studied here, the relatively modest intrachain polaron coherence lengths we measure are a direct result of the fact that the F_4TCNQ anion always resides within 1 nm of the polaron, so that polaron coherence is always limited by the local Coulombic interaction with the anion, independent of how well ordered the P3HT crystallites are. Thus, although F_4TCNQ is certainly a useful molecular dopant for studying polaron behavior in conjugated polymers, the relatively strong Coulombic interaction it partakes in puts a fundamental limit on the degree of polaron coherence for this polymer−dopant combination. Fortunately, these issues can be avoided with the use of other dopants that better screen the polaron−counterion Coulombic interaction.[13,14]

We close by noting that in many ways measuring the electric field landscape in doped semiconducting materials is precisely the kind of application that vibrational Stark probes were designed to explore. The nitrile groups that make this kind of analysis possible are commonly added to p-type dopants to make them stronger oxidizers. Thus, application of dopants as VSE probes is a natural use for these molecules. Although the current generation of nitrile-containing dopants like F_4TCNQ were not designed to be used this way, it is exciting to imagine an entirely new class of p-type dopants that could be specifically engineered to fulfill the dual roles of being strong oxidizers that also map the electric fields from polarons in these materials. For these reasons, we are optimistic that the VSE will become a more generally applied principle in this area for probing the Coulombic interactions in doped conjugated polymers.

■ ASSOCIATED CONTENT

Supporting Information

The Supporting Information is available free of charge at https://pubs.acs.org/doi/10.1021/acs.chemmater.1c02934.

Detailed information about materials used, fabrication and doping of polymer films, FTIR measurements, peak fitting of the F_4TCNQ C≡N vibrational spectra, tabulated fitting parameters, dopant−polaron Coulombic modeling, and GIWAXS measurements of doped polymer films (PDF)

■ AUTHOR INFORMATION

Corresponding Author

Benjamin J. Schwartz − *Department of Chemistry and Biochemistry, University of California, Los Angeles, Los Angeles, California 90095-1569, United States;* orcid.org/0000-0003-3257-9152; Email: schwartz@chem.ucla.edu

Authors

Dane A. Stanfield − *Department of Chemistry and Biochemistry, University of California, Los Angeles, Los Angeles, California 90095-1569, United States*

Zerina Mehmedović − *Department of Chemistry and Biochemistry, University of California, Los Angeles, Los Angeles, California 90095-1569, United States*

Complete contact information is available at: https://pubs.acs.org/10.1021/acs.chemmater.1c02934

Notes

The authors declare no competing financial interest.

■ ACKNOWLEDGMENTS

This work was supported by the National Science Foundation under Grants CHE-2003755 and DMR-2105896.

■ REFERENCES

(1) Kuik, M.; Wetzelaer, G. J. A.; Nicolai, H. T.; Craciun, N. I.; De Leeuw, D. M.; Blom, P. W. 25th anniversary article: Charge transport and recombination in polymer light-emitting diodes. *Adv. Mater.* **2014**, *26*, 512−531.

(2) Dou, L.; You, J.; Hong, Z.; Xu, Z.; Li, G.; Street, R. A.; Yang, Y. 25th anniversary article: A decade of organic/polymeric photovoltaic research. *Adv. Mater.* **2013**, *25*, 6642−6671.

(3) Russ, B.; Glaudell, A.; Urban, J. J.; Chabinyc, M. L.; Segalman, R. A. Organic Thermoelectric Materials for Energy Harvesting and Temperature Control. *Nat. Rev. Mater.* **2016**, *1*, 1−14.

(4) Cowart, J. S.; Liman, C.; Garnica, A.; Page, Z. A.; Lim, E.; Zope, R. R.; Baruah, T.; Hawker, C. J.; Chabinyc, M. L. Donor-fullerene

dyads for energy cascade organic solar cells. *Inorg. Chim. Acta* **2017**, *468*, 192−202.
(5) Hou, L.; Zhang, X.; Cotella, G. F.; Carnicella, G.; Herder, M.; Schmidt, B. M.; Pätzel, M.; Hecht, S.; Cacialli, F.; Samorì, P. Optically switchable organic light-emitting transistors. *Nat. Nanotechnol.* **2019**, *14*, 347−353.
(6) Scholes, D. T.; Yee, P. Y.; Lindemuth, J. R.; Kang, H.; Onorato, J.; Ghosh, R.; Luscombe, C. K.; Spano, F. C.; Tolbert, S. H.; Schwartz, B. J. The Effects of Crystallinity on Charge Transport and the Structure of Sequentially Processed F4TCNQ-Doped Conjugated Polymer Films. *Adv. Funct. Mater.* **2017**, *27*, 1702654.
(7) Chew, A. R.; Ghosh, R.; Shang, Z.; Spano, F. C.; Salleo, A. Sequential Doping Reveals the Importance of Amorphous Chain Rigidity in Charge Transport of Semi-Crystalline Polymers. *J. Phys. Chem. Lett.* **2017**, *8*, 4974−4980.
(8) Ghosh, R.; Chew, A. R.; Onorato, J.; Pakhnyuk, V.; Luscombe, C. K.; Salleo, A.; Spano, F. C. Spectral Signatures and Spatial Coherence of Bound and Unbound Polarons in P3HT Films: Theory Versus Experiment. *J. Phys. Chem. C* **2018**, *122*, 18048−18060.
(9) Ghosh, R.; Luscombe, C. K.; Hambsch, M.; Mannsfeld, S. C. B.; Salleo, A.; Spano, F. C. Anisotropic Polaron Delocalization in Conjugated Homopolymers and Donor−Acceptor Copolymers. *Chem. Mater.* **2019**, *31*, 7033−7045.
(10) Ghosh, R.; Spano, F. C. Excitons and Polarons in Organic Materials. *Acc. Chem. Res.* **2020**, *53*, 2201−2211.
(11) Kiefer, D.; Kroon, R.; Hofmann, A. I.; Sun, H.; Liu, X.; Giovannitti, A.; Stegerer, D.; Cano, A.; Hynynen, J.; Yu, L.; et al. Double doping of conjugated polymers with monomer molecular dopants. *Nat. Mater.* **2019**, *18*, 149−155.
(12) Scholes, D. T.; Yee, P. Y.; Mckeown, G. R.; Li, S.; Kang, H.; Lindemuth, R.; Xia, X.; King, S. C.; Seferos, D. S.; Tolbert, S. H.; et al. Designing Conjugated Polymers for Molecular Doping: The Roles of Crystallinity, Swelling, and Conductivity in Sequentially-Doped Selenophene-Based Copolymers. *Chem. Mater.* **2019**, *31*, 73−82.
(13) Aubry, T. J.; Axtell, J. C.; Basile, V. M.; Winchell, K. J.; Lindemuth, J. R.; Porter, T. M.; Liu, J.-Y.; Alexandrova, A. N.; Kubiak, C. P.; Tolbert, S. H.; Spokoyny, A. M.; Schwartz, B. J. Dodecaborane-Based Dopants Designed to Shield Anion Electrostatics Lead to Increased Carrier Mobility in a Doped Conjugated Polymer. *Adv. Mater.* **2019**, *31*, 1805647.
(14) Aubry, T. J.; Winchell, K. J.; Salamat, C. Z.; Basile, V. M.; Lindemuth, J. R.; Stauber, J. M.; Axtell, J. C.; Kubena, R. M.; Phan, M. D.; Bird, M. J.; et al. Tunable Dopants with Intrinsic Counterion Separation Reveal the Effects of Electron Affinity on Dopant Intercalation and Free Carrier Production in Sequentially Doped Conjugated Polymer Films. *Adv. Funct. Mater.* **2020**, *30*, 2001800.
(15) Stanfield, D. A.; Wu, Y.; Tolbert, S. H.; Schwartz, B. J. Controlling the Formation of Charge Transfer Complexes in Chemically Doped Semiconducting Polymers. *Chem. Mater.* **2021**, *33*, 2343.
(16) Pingel, P.; Zhu, L.; Park, K. S.; Vogel, J.-O.; Janietz, S.; Kim, E.-G.; Rabe, J. P.; Brédas, J.-L.; Koch, N. Charge-Transfer Localization in Molecularly Doped Thiophene-Based Donor Polymers. *J. Phys. Chem. Lett.* **2010**, *1*, 2037−2041.
(17) Zhu, L.; Kim, E.-G.; Yi, Y.; Brédas, J.-L. Charge Transfer in Molecular Complexes with 2,3,5,6-Tetrafluoro-7,7,8,8-tetracyanoquinodimethane (F 4 -TCNQ): A Density Functional Theory Study. *Chem. Mater.* **2011**, *23*, 5149−5159.
(18) Ghani, F.; Opitz, A.; Pingel, P.; Heimel, G.; Salzmann, I.; Frisch, J.; Neher, D.; Tsami, A.; Scherf, U.; Koch, N. Charge transfer in and conductivity of molecularly doped thiophene-based copolymers. *J. Polym. Sci., Part B: Polym. Phys.* **2015**, *53*, 58−63.
(19) Thomas, E. M.; Davidson, E. C.; Katsumata, R.; Segalman, R. A.; Chabinyc, M. L. Branched Side Chains Govern Counterion Position and Doping Mechanism in Conjugated Polythiophenes. *ACS Macro Lett.* **2018**, *7*, 1492−1497.
(20) Neelamraju, B.; Watts, K. E.; Pemberton, J. E.; Ratcliff, E. L. Correlation of Coexistent Charge Transfer States in F 4 TCNQ-Doped P3HT with Microstructure. *J. Phys. Chem. Lett.* **2018**, *9*, 6871−6877.
(21) Jacobs, I. E.; Cendra, C.; Harrelson, T. F.; Bedolla Valdez, Z. I.; Faller, R.; Salleo, A.; Moulé, A. J. Polymorphism controls the degree of charge transfer in a molecularly doped semiconducting polymer. *Mater. Horiz.* **2018**, *5*, 655−660.
(22) Watts, K. E.; Neelamraju, B.; Ratcliff, E. L.; Pemberton, J. E. Stability of Charge Transfer States in F 4 TCNQ-Doped P3HT. *Chem. Mater.* **2019**, *31*, 6986−6994.
(23) Kondratenko, K.; Boussoualem, Y.; Singh, D. P.; Visvanathan, R.; Duncan, A. E.; Clark, N. A.; Legrand, C.; Daoudi, A. Molecular p-doping in organic liquid crystalline semiconductors: influence of the charge transfer complex on the properties of mesophase and bulk charge transport. *Phys. Chem. Chem. Phys.* **2019**, *21*, 18686−18698.
(24) Thomas, A. K.; Datko, B. D.; Grey, J. K. Charge Transfer Doping of Conjugated Polymers with Large Vibrational Activities: Insights into the Regime of Partial Charge Transfer. *J. Phys. Chem. C* **2020**, *124*, 2137−2145.
(25) Zapata-Arteaga, O.; Dörling, B.; Perevedentsev, A.; Martín, J.; Reparaz, J. S.; Campoy-Quiles, M. Closing the Stability-Performance Gap in Organic Thermoelectrics by Adjusting the Partial to Integer Charge Transfer Ratio. *Macromolecules* **2020**, *53*, 609−620.
(26) Hase, H.; O'Neill, K.; Frisch, J.; Opitz, A.; Koch, N.; Salzmann, I. Unraveling the Microstructure of Molecularly Doped Poly(3-hexylthiophene) by Thermally Induced Dedoping. *J. Phys. Chem. C* **2018**, *122*, 25893−25899.
(27) Chattopadhyay, A.; Boxer, S. G. Vibrational Stark Effect Spectroscopy. *J. Am. Chem. Soc.* **1995**, *117*, 1449−1450.
(28) Andrews, S. S.; Boxer, S. G. Vibrational Stark effects of nitriles. I. Methods and experimental results. *J. Phys. Chem. A* **2000**, *104*, 11853−11863.
(29) Park, E. S.; Thomas, M. R.; Boxer, S. G. Vibrational Stark Spectroscopy of NO Bound to Heme: Effects of Protein Electrostatic Fields on the NO Stretch Frequency. *J. Am. Chem. Soc.* **2000**, *122*, 12297−12303.
(30) Suydam, I. T.; Boxer, S. G. Vibrational Stark Effects Calibrate the Sensitivity of Vibrational Probes for Electric Fields in Proteins. *Biochemistry* **2003**, *42*, 12050−12055.
(31) Brewer, S. H.; Franzen, S. A quantitative theory and computational approach for the vibrational Stark effect. *J. Chem. Phys.* **2003**, *119*, 851−858.
(32) Dalosto, S. D.; Vanderkooi, J. M.; Sharp, K. A. Vibrational Stark Effects on Carbonyl, Nitrile, and Nitrosyl Compounds Including Heme Ligands, CO, CN, and NO, Studied with Density Functional Theory. *J. Phys. Chem. B* **2004**, *108*, 6450−6457.
(33) Sigala, P. A.; Fafarman, A. T.; Bogard, P. E.; Boxer, S. G.; Herschlag, D. Do Ligand Binding and Solvent Exclusion Alter the Electrostatic Character within the Oxyanion Hole of an Enzymatic Active Site? *J. Am. Chem. Soc.* **2007**, *129*, 12104−12105.
(34) Hu, W.; Webb, L. J. Direct Measurement of the Membrane Dipole Field in Bicelles Using Vibrational Stark Effect Spectroscopy. *J. Phys. Chem. Lett.* **2011**, *2*, 1925−1930.
(35) Fried, S. D.; Boxer, S. G. Measuring Electric Fields and Noncovalent Interactions Using the Vibrational Stark Effect. *Acc. Chem. Res.* **2015**, *48*, 998−1006.
(36) Slocum, J. D.; Webb, L. J. Nitrile Probes of Electric Field Agree with Independently Measured Fields in Green Fluorescent Protein Even in the Presence of Hydrogen Bonding. *J. Am. Chem. Soc.* **2016**, *138*, 6561−6570.
(37) Adhikary, R.; Zimmermann, J.; Romesberg, F. E. Transparent Window Vibrational Probes for the Characterization of Proteins With High Structural and Temporal Resolution. *Chem. Rev.* **2017**, *117*, 1927−1969.
(38) Slocum, J. D.; Webb, L. J. Measuring Electric Fields in Biological Matter Using the Vibrational Stark Effect of Nitrile Probes. *Annu. Rev. Phys. Chem.* **2018**, *69*, 253−271.
(39) Martin, D. R.; Matyushov, D. V. Why are Vibrational Lines Narrow in Proteins? *J. Phys. Chem. Lett.* **2020**, *11*, 5932−5937.

https://doi.org/10.1021/acs.chemmater.1c02934
Chem. Mater. XXXX, XXX, XXX−XXX

(40) Li, Y.; Zolotavin, P.; Doak, P.; Kronik, L.; Neaton, J. B.; Natelson, D. Interplay of Bias-Driven Charging and the Vibrational Stark Effect in Molecular Junctions. *Nano Lett.* **2016**, *16*, 1104−1109.
(41) Staffa, J. K.; Lorenz, L.; Stolarski, M.; Murgida, D. H.; Zebger, I.; Utesch, T.; Kozuch, J.; Hildebrandt, P. Determination of the Local Electric Field at Au/SAM Interfaces Using the Vibrational Stark Effect. *J. Phys. Chem. C* **2017**, *121*, 22274−22285.
(42) Ge, A.; Videla, P. E.; Lee, G. L.; Rudshteyn, B.; Song, J.; Kubiak, C. P.; Batista, V. S.; Lian, T. Interfacial Structure and Electric Field Probed by in Situ Electrochemical Vibrational Stark Effect Spectroscopy and Computational Modeling. *J. Phys. Chem. C* **2017**, *121*, 18674−18682.
(43) Zwaschka, G.; Wolf, M.; Campen, R. K.; Tong, Y. A Microscopic Model of the Electrochemical Vibrational Stark Effect: Understanding VSF Spectroscopy of (bi)Sulfate on Pt(111). *Surf. Sci.* **2018**, *678*, 78−85.
(44) Pfisterer, J. H. K.; Zhumaev, U. E.; Cheuquepan, W.; Feliu, J. M.; Domke, K. F. Stark effect or coverage dependence? Disentangling the EC-SEIRAS vibrational shift of sulfate on Au(111). *J. Chem. Phys.* **2019**, *150*, 041709.
(45) Mani, T.; Grills, D. C.; Miller, J. R. Vibrational Stark Effects To Identify Ion Pairing and Determine Reduction Potentials in Electrolyte-Free Environments. *J. Am. Chem. Soc.* **2015**, *137*, 1136−1140.
(46) Hack, J.; Grills, D. C.; Miller, J. R.; Mani, T. Identification of Ion-Pair Structures in Solution by Vibrational Stark Effects. *J. Phys. Chem. B* **2016**, *120*, 1149−1157.
(47) Donon, J.; Habka, S.; Vaquero-Vara, V.; Brenner, V.; Mons, M.; Gloaguen, E. Electronic Stark Effect in Isolated Ion Pairs. *J. Phys. Chem. Lett.* **2019**, *10*, 7458−7462.
(48) Drexler, C. I.; Cracchiolo, O. M.; Myers, R. L.; Okur, H. I.; Serrano, A. L.; Corcelli, S. A.; Cremer, P. S. Local Electric Fields in Aqueous Electrolytes. *J. Phys. Chem. B* **2021**, *125*, 8484−8493.
(49) Cho, M. Vibrational solvatochromism and electrochromism: Coarse-grained models and their relationships. *J. Chem. Phys.* **2009**, *130*, 094505.
(50) Kang, H.; Maurais, J.; Park, Y.; Ayotte, P.; Kang, H. Electric Field Effect on Condensed-Phase Molecular Systems. VIII. Vibrational Stark Effect and Dipolar Inversion in a Carbon Monoxide Crystal. *J. Phys. Chem. C* **2019**, *123*, 31262−31271.
(51) Kang, H.; Park, Y.; Shin, S.; Kang, H. Electric Field Effect on Condensed-Phase Molecular Systems. X. Interconversion Dynamics and Vibrational Stark Effect of Hydrogen Chloride Clusters in an Argon Matrix. *J. Phys. Chem. B* **2020**, *124*, 4581−4589.
(52) Scholes, D. T.; Hawks, S. A.; Yee, P. Y.; Wu, H.; Lindemuth, J. R.; Tolbert, S. H.; Schwartz, B. J. Overcoming Film Quality Issues for Conjugated Polymers Doped with F4TCNQ by Solution Sequential Processing: Hall Effect, Structural, and Optical Measurements. *J. Phys. Chem. Lett.* **2015**, *6*, 4786−4793.
(53) Fontana, M. T.; Stanfield, D. A.; Scholes, D. T.; Winchell, K. J.; Tolbert, S. H.; Schwartz, B. J. Evaporation vs Solution Sequential Doping of Conjugated Polymers: F 4 TCNQ Doping of Micrometer-Thick P3HT Films for Thermoelectrics. *J. Phys. Chem. C* **2019**, *123*, 22711−22724.
(54) Yee, P. Y.; Scholes, D. T.; Schwartz, B. J.; Tolbert, S. H. Dopant-Induced Ordering of Amorphous Regions in Regiorandom P3HT. *J. Phys. Chem. Lett.* **2019**, *10*, 4929−4934.
(55) Voss, M. G.; Scholes, D. T.; Challa, J. R.; Schwartz, B. J. Ultrafast transient absorption spectroscopy of doped P3HT films: Distinguishing free and trapped polarons. *Faraday Discuss.* **2019**, *216*, 339−362.
(56) Doubina, N.; Ho, A.; Jen, A. K-Y; Luscombe, C. K. Effect of Initiators on the Kumada Catalyst-Transfer Polycondensation Reaction. *Macromolecules* **2009**, *42*, 7670−7677.
(57) Meneghetti, M.; Pecile, C. Charge−transfer organic crystals: Molecular vibrations and spectroscopic effects of electron−molecular vibration coupling of the strong electron acceptor TCNQF 4. *J. Chem. Phys.* **1986**, *84*, 4149−4162.
(58) Méndez, H.; Heimel, G.; Winkler, S.; Frisch, J.; Opitz, A.; Sauer, K.; Wegner, B.; Oehzelt, M.; Röthel, C.; Duhm, S.; et al. Charge-transfer crystallites as molecular electrical dopants. *Nat. Commun.* **2015**, *6*, 8560.
(59) Aziz, E. F.; Vollmer, A.; Eisebitt, S.; Eberhardt, W.; Pingel, P.; Neher, D.; Koch, N. Localized Charge Transfer in a Molecularly Doped Conducting Polymer. *Adv. Mater.* **2007**, *19*, 3257−3260.
(60) Kang, K.; Watanabe, S.; Broch, K.; Sepe, A.; Brown, A.; Nasrallah, I.; Nikolka, M.; Fei, Z.; Heeney, M.; Matsumoto, D.; et al. 2D Coherent Charge Transport in Highly Ordered Conducting Polymers Doped by Solid State Diffusion. *Nat. Mater.* **2016**, *15*, 896−903.
(61) Patel, S. N.; Glaudell, A. M.; Peterson, K. A.; Thomas, E. M.; O'Hara, K. A.; Lim, E.; Chabinyc, M. L. Morphology Controls the Thermoelectric Power Factor of a Doped Semiconducting Polymer. *Sci. Adv.* **2017**, *3*, 24−26.
(62) Hamidi-Sakr, A.; Biniek, L.; Bantignies, J. L.; Maurin, D.; Herrmann, L.; Leclerc, N.; Lévêque, P.; Vijayakumar, V.; Zimmermann, N.; Brinkmann, M. A Versatile Method to Fabricate Highly In-Plane Aligned Conducting Polymer Films with Anisotropic Charge Transport and Thermoelectric Properties: The Key Role of Alkyl Side Chain Layers on the Doping Mechanism. *Adv. Funct. Mater.* **2017**, *27*, 1700173.
(63) Lim, E.; Peterson, K. A.; Su, G. M.; Chabinyc, M. L. Thermoelectric Properties of Poly(3-hexylthiophene) (P3HT) Doped with 2,3,5,6-Tetrafluoro-7,7,8,8-tetracyanoquinodimethane (F4TCNQ) by Vapor-Phase Infiltration. *Chem. Mater.* **2018**, *30*, 998−1010.
(64) Lim, E.; Glaudell, A. M.; Miller, R.; Chabinyc, M. L. The Role of Ordering on the Thermoelectric Properties of Blends of Regioregular and Regiorandom Poly(3-hexylthiophene). *Advanced Electronic Materials* **2019**, *5*, 1800915.
(65) Untilova, V.; Biskup, T.; Biniek, L.; Vijayakumar, V.; Brinkmann, M. Control of Chain Alignment and Crystallization Helps Enhance Charge Conductivities and Thermoelectric Power Factors in Sequentially Doped P3HT:F 4 TCNQ Films. *Macromolecules* **2020**, *53*, 2441−2453.
(66) Haworth, N. L.; Lu, J.; Vo, N.; Le, T. H.; Thompson, C. D.; Bond, A. M.; Martin, L. L. Diagnosis of the Redox Levels of TCNQF 4 Compounds Using Vibrational Spectroscopy. *ChemPlusChem.* **2014**, *79*, 962−972.
(67) Pingel, P.; Neher, D. Comprehensive picture of p-type doping of P3HT with the molecular acceptor F4TCNQ. *Phys. Rev. B: Condens. Matter Mater. Phys.* **2013**, *87*, 115209.
(68) Vijayakumar, V.; Zhong, Y.; Untilova, V.; Bahri, M.; Herrmann, L.; Biniek, L.; Leclerc, N.; Brinkmann, M. Bringing Conducting Polymers to High Order- Toward Conductivities beyond 10 5 S cm-1 and Thermoelectric Power Factors of 2 mW m-1 K. *Adv. Energy Mater.* **2019**, *9*, 1900266.
(69) Vijayakumar, V.; Zaborova, E.; Biniek, L.; Zeng, H.; Herrmann, L.; Carvalho, A.; Boyron, O.; Leclerc, N.; Brinkmann, M. Effect of Alkyl Side Chain Length on Doping Kinetics, Thermopower, and Charge Transport Properties in Highly Oriented F 4 TCNQ-Doped PBTTT Films. *ACS Appl. Mater. Interfaces* **2019**, *11*, 4942−4953.
(70) Vijayakumar, V.; Durand, P.; Zeng, H.; Untilova, V.; Herrmann, L.; Algayer, P.; Leclerc, N.; Brinkmann, M. Influence of dopant size and doping method on the structure and thermoelectric properties of PBTTT films doped with F6TCNNQ and F4TCNQ. *J. Mater. Chem. C* **2020**, *8*, 16470−16482.

https://doi.org/10.1021/acs.chemmater.1c02934
Chem. Mater. XXXX, XXX, XXX−XXX